Since January 2020 Elsevier has created a COVID-19 resource centre with free information in English and Mandarin on the novel coronavirus COVID-19. The COVID-19 resource centre is hosted on Elsevier Connect, the company's public news and information website.

Biosensors and Bioelectronics 195 (2022) 113646

Contents lists available at ScienceDirect

Biosensors and Bioelectronics

journal homepage: www.elsevier.com/locate/bios

A smartphone-based visual biosensor for CRISPR-Cas powered SARS-CoV-2 diagnostics

Long Ma [a,*,1], Lijuan Yin [a,1], Xiaoyan Li [b,1], Si Chen [a,1], Lei Peng [a], Guozhen Liu [c], Shengying Ye [d], Wenlu Zhang [a], Shuli Man [a]

[a] State Key Laboratory of Food Nutrition and Safety, Key Laboratory of Industrial Microbiology, Ministry of Education, Tianjin Key Laboratory of Industry Microbiology, National and Local United Engineering Lab of Metabolic Control Fermentation Technology, China International Science and Technology Cooperation Base of Food Nutrition/Safety and Medicinal Chemistry, College of Biotechnology, Tianjin University of Science & Technology, Tianjin, 300457, China
[b] Institute of Pathogen Biology, Tianjin Centers for Disease Control and Prevention, Tianjin, 300011, China
[c] School of Life and Health Sciences, The Chinese University of Hong Kong, Shenzhen, 518172, China
[d] Pharmacy Department, The 983rd, Hospital of the Joint Logistics Support Force of the Chinese People's Liberation Army, Tianjin, 300142, China

ARTICLE INFO

Keywords:
CRISPR-Cas12a
Gold nanoparticles
SARS-CoV-2 detection
Smartphone-based diagnostics
Visual biosensor
Clinical samples

ABSTRACT

The pandemic of coronavirus disease 2019 (COVID-19) resulted from novel severe acute respiratory syndrome coronavirus 2 (SARS-CoV-2) has become a worldwide concern. It is imperative to develop rapid, sensitive, and specific biosensing methods. Herein, we developed a CRISPR-Cas12a powered visual biosensor with a smartphone readout for ultrasensitive and selective detection of SARS-CoV-2. Simply, the SARS-CoV-2 derived nucleic acids triggered CRISPR-Cas12a based indiscriminate degradation of a single-stranded DNA that was supposed to link two gold nanoparticles, inducing the dis-aggregation of gold nanoparticles and thus generating observable color changes. This change can be readily distinguished by naked eyes as well as a smartphone with a Color Picker App. The proposed biosensor was successfully applied to detect SARS-CoV-2 gene in synthetic vectors, transcribed RNA and SARS-CoV-2 pseudoviruses. It rendered "single copy resolution" as evidenced by the 1 copy/μL limit of detection of pseudoviruses with no cross-reactivity. When the developed biosensor was challenged with SARS-CoV-2 clinical bio-samples, it provided 100% agreement (both positive and negative) with qPCR results. The sample-to-result time was roughly 90 min. Our work provides a novel and robust technology for ultrasensitive detection of SARS-CoV-2 that could be used clinically.

1. Introduction

A novel coronavirus, termed as SARS-CoV-2, was isolated from the patients' samples in 2020 and was soon identified as the pathogen causing the COVID-19, a newly spreading human infectious disease (Zhu et al., 2020). In short, the high contagiousness and rapid transmission of SARS-CoV-2 create huge challenge for regular epidemic prevention and control. All these require prompt identification of pathogens with ease and accuracy. Quantitative real-time PCR (qPCR) is the most popular approach for pathogenic nucleic acid detection and thus has been officially approved by the WHO (World Health Organization) as standardized method for COVID-19 diagnostics (Corman et al., 2020).

It is known that the clustered regularly interspaced short palindromic repeats (CRISPR) together with CRISPR-associated genes (Cas), an adaptive immune system, protects bacteria and archaea against invading DNA and phages (Barrangou et al., 2007). CRISPR-Cas systems also have demonstrated huge potentials in biosensing (Morales-Narváez and Dincer, 2020; Li et al., 2019a,b; Kaminski et al., 2021; Wu et al., 2021; Yin et al., 2021). Recently, certain CRISPR-Cas systems including Cas13a and Cas12a are found to own nonspecific nucleic acid cutting activities (also named *trans*-cleavage) upon the recognition of target sequence by crRNA (CRISPR RNA) (Abudayyeh et al., 2016; Chen et al., 2018). Such *trans*-cleavage activity provides the unique basis for the detection of nucleic acids with high sensitivity and selectivity, by which detection platforms including SHERLOCK (Gootenberg et al., 2017), DETECTR (Chen et al., 2018), HOLMES (Li et al., 2018) and some other variants (Chen et al., 2020; Peng et al., 2020; Zhou et al., 2020) have been fabricated. Several groups have reported SARS-CoV-2 detection by

* Corresponding author.
E-mail addresses: malong@tust.edu.cn, woshimalong1983@163.com (L. Ma).
[1] The first four authors contributed equally and shared the joint first authorship.

https://doi.org/10.1016/j.bios.2021.113646
Received 15 March 2021; Received in revised form 4 September 2021; Accepted 14 September 2021
Available online 23 September 2021

utilizing CRISPR-Cas13a or CRISPR-Cas12a coupled with either fluorescent signal readouts or colorimetric signal readouts in paper lateral flow assays (Broughton et al., 2020). However, the sensitivity and selectivity of these methods require further improvement in order to achieve satisfied performance in detection of clinical samples. For example, Broughton and co-work performed CRISPR-Cas12a based detection of SARS-CoV-2 with both fluorescent and lateral flow readouts. The results showed that both had LOD values of 10 copies/μL with a detection range from 10 to 2500 copies/μL (Broughton et al., 2020). Similarly, the LOD of CRISPR-Cas13a fluorescent SARS-CoV-2 assay was 42 copies/reaction (Patchsung et al., 2020). This indicated that a sample with viral concentration less than the LOD values was very likely to be incorrectly identified. It is prominent to develop rapid, ultrasensitive and specific detection strategies for SARS-CoV-2 detection.

The applications of plasmonic gold nanoparticles (AuNPs) in biosensing received an increasing deal of attention (Ahmadivand et al., 2021; Chang et al., 2019; Liu and Lu, 2006; Jans and Huo, 2012). Moreover, the power of smartphones such as cameras, interactivity, portability demonstrates huge feasibility in biosensing. The coupling of smartphone with biosensing enables field-deployable and user-friendly analytical devices (Quesada-González and Merkoçi, 2017). In this study, a novel CRISPR-Cas12a powered visual biosensor for ultrasensitive SARS-CoV-2 detection was developed.

2. Materials and methods

2.1. Materials

EnGen® Lba Cas12a was bought from New England Biolabs (USA). Commercial plasmids containing SARS-CoV-2 N gene fragment and SARS-CoV N gene, respectively were synthesized by Generay Biotech Co., Ltd (China). Ribonuclease inhibitor was purchased from Beyotime Biotechnology (China). M-MLV Reverse Transcriptase and dNTP master mix were obtained from Promega (USA). Others were listed in the supplementary information.

2.2. Preparation of crRNA

The crRNA synthesis was strictly conducted as our previous work (Peng et al., 2020).

2.3. Study on the feasibility of CRISPR-Cas12 assay for nucleic acid detection

The plasmid (100 pM) containing N gene fragment of SARS-CoV-2 was amplified by PCR. The ssDNA reporter was doubly labeled with 5′ 6-FAM (Fluorescein) and 3’ BHQ1 (Black Hole Quencher 1). The assay contained 15 nM LbCas12a, 12.5 nM crRNA, 5 μL PCR product and 200 nM ssDNA reporter in a 100 μL reaction with NEBuffer 2.1. The fluorescence was detected by a Tecan plate reader with 484 nm excitation and 529 nm emission wavelengths at 37 °C.

2.4. CRISPR-Cas12a powered visual biosensor

For a typical CRISPR-Cas12a powered visual biosensor, a reaction containing 200 nM LbCas12a, 250 nM crRNA, 25 nM linker ssDNA, and varying concentrations of target DNA was incubated in HEPES buffer (5 mM HEPES, 150 mM NaCl, 10 mM $MgCl_2$, pH 7.6) at 37 °C for 15 min, followed by a 5 min deactivation process at 65 °C. 50 μL of this reaction was mixed with 25 μL AuNPs-DNA1 and 25 μL AuNPs-DNA2 solution (both 5.0 nM) and maintained at 37 °C for 5 min. Each sample was precipitated after centrifugation (3500 rpm for 1 min). The color of the supernatant and the UV–Vis absorbance (A_{526}) were then recorded.

2.5. The smartphone readout of CRISPR-Cas12a powered visual biosensor for SARS-CoV-2 detection

The RGB image of CRISPR-Cas12a powered visual biosensor taken under sunlight or common daylight lamp was converted to a greyscale image that was then analyzed offline using the Color Picker App. The RGB color model is an additive color model (Arai et al., 2018) in which red, green, and blue light are added together in various ways to reproduce a broad array of colors. The name of the model comes from the initials of the three additive primary colors, red, green and blue. The user identified the regions of interest in the images by overlaying a pre-set circle onto the tubes. The image was then subjected to analysis. Within each of the user-selected area, the server generated a list of information including HSL (Hue, Saturation, Lightness) (Fig. S4), the lightness value was then extracted for use.

2.6. Clinical bio-sample analysis

The study was officially approved by the ethical review committee of Tianjin Centers for Disease Control and Prevention (CDC). De-identified throat swabs samples from confirmed cases of COVID-19 and healthy individuals who were tested positive and negative for SARS-CoV-2 were obtained by the Tianjin centers for Disease Control and Prevention. Positive samples were officially verified. The obtained RNA samples were reversely transcribed into the cDNA, followed by PCR amplification. Then the PCR products were transferred to a new tube for CRISPR-Cas12a powered visual biosensor (Section 2.5).

2.7 Other methods used in the study were described in the supplementary information.

3. Results and discussion

3.1. The principle of CRISPR-Cas12a powered visual biosensor for SARS-CoV-2 detection with a smartphone readout

The principle of the designed biosensor was depicted in Fig. 1. Specifically, viral RNA is extracted, reversely transcribed and amplified using SARS-CoV-2 N gene specific primers to obtain double-stranded (ds) DNA amplicons. Upon the recognition of the dsDNA amplicons (also called target dsDNA) by Cas12a-crRNA complex, the indiscriminate *trans*-cleavage of ssDNA can be initiated. If this ssDNA is doubly labeled with a fluorophore (F) at 5′ and a quencher (Q) at 3’ ends, such cleavage breaks their close vicinity, resulting in a dequenching state. This gives rise to enhanced fluorescent signals for quantitative analysis of target dsDNA (Fig. 1A). Besides, we design a linker ssDNA, which is able to hybridize with pre-made AuNPs-DNA probe pairs via complementary base pairing. When the reaction is devoid of the target dsDNA, the linker ssDNA remains uncut and the AuNPs probes would experience a DNA hybridization induced aggregation and thus be “pulled down”. This close vicinity of cross-linked AuNPs causes interparticle plasmon coupling, giving rise to a red shift in their absorbance, and hence the solution represents purple color and colorless after centrifugation (Zhao et al., 2008; Zagorovsky and Chan, 2013). In the presence of target dsDNA, the *trans*-cleavage activity of Cas12a is activated and the linker ssDNA is cut off, causing the dis-aggregation of AuNPs. The solution remains red color even after mild centrifugation. This “turn-on” color change could be readily discerned by naked eyes and also be captured by a smartphone installed with Color Picker App (Fig. 1B). Thus, SARS-CoV-2 is detected based on the changes of color. Fig. 1C depicted the required time for each step of the proposed biosensor and Fig. 1D showed the nucleic acids sequences used in this study.

3.2. The feasibility of CRISPR-Cas12a trans-cleavage for detecting SARS-CoV-2 in synthetic gene vector and transcribed virus-specific RNA

By using the published genome sequence of SARS-CoV-2

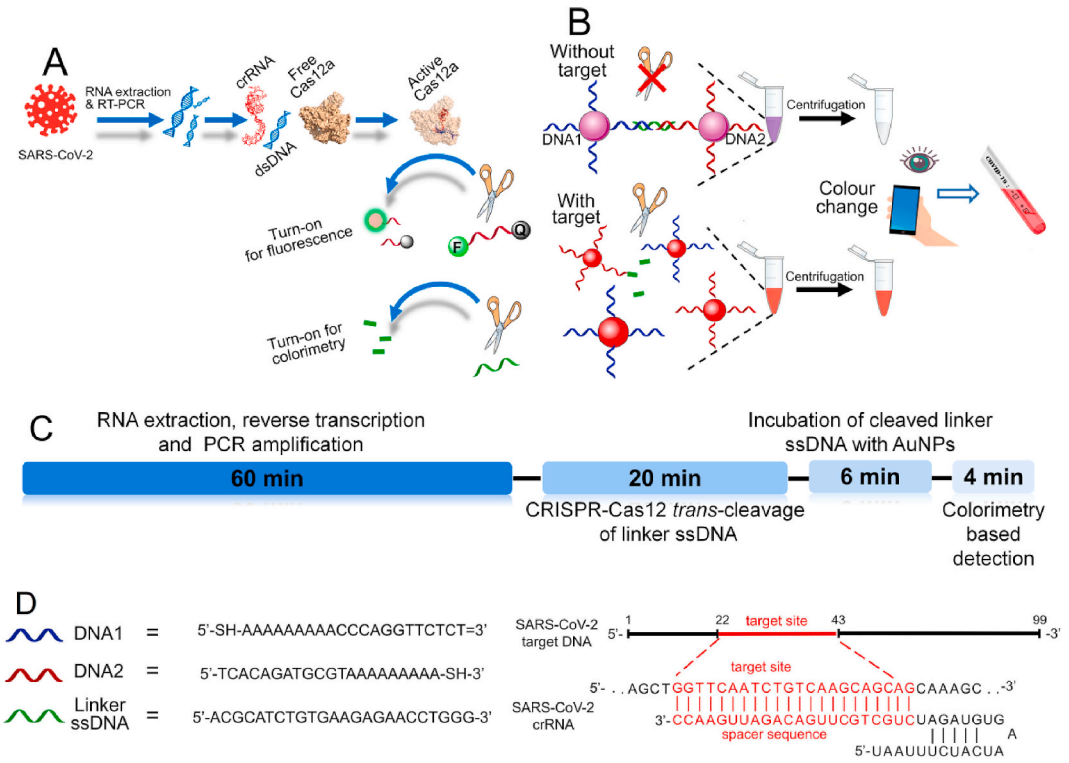

Fig. 1. The *trans*-cleavage of CRISPR-Cas12a can be utilized to devise fluorescent and colorimetric biosensors for SARS-CoV-2 detection. (A) The scheme of SARS-CoV-2 detection by utilizing the *trans*-cleavage of CRISPR-Cas12a upon the recognition of SARS-CoV-2 specific amplicons. The ssDNA reporter is doubly labeled with FAM fluorophore and BHQ1 at the 5′ and 3′ ends, respectively. (B) The principle of CRISPR-Cas12a powered visual biosensor with a smartphone readout. (C) Estimated time duration for each step of the proposed biosensor. (D) The sequences used in this study. The target site for used for SARS-CoV-2 detection is highlighted in red. (For interpretation of the references to color in this figure legend, the reader is referred to the Web version of this article.)

(NC_045512.2), we designed crRNA corresponding to part of the nucleocapsid (N) gene, as recommended by Chinese CDC and US CDC for SARS-CoV-2 detection. The crRNA target was shown in Fig. S1A. All SARS-CoV-2 sequences uploaded to GISAID database were analyzed. The crRNA and the PCR primers we designed were highly conserved, suggesting that our selected crRNA and primers can be used for all known SARS-CoV-2 genomes. Meanwhile, the sequences of the crRNA and PCR primers were aligned to some other related coronaviruses including severe acute respiratory syndrome (SARS-CoV), middle east respiratory syndrome (MERS-CoV), and human coronaviruses (Human-CoV) to evaluate their specificity, and found that our design was highly specific for SARS-CoV-2 (Fig. S1B).

To test the feasibility of our proposed CRISPR-Cas12a based detection, we performed some preliminary experiments on the plasmid containing N gene fragment of SARS-CoV-2. The results indicated that the *trans*-cleavage of Cas12a was triggered only when the target N gene dsDNA amplicons (Fig. S1C) and crRNA were both present, which was evidenced by the significantly increased fluorescence (FL). When the correct crRNA or target dsDNA amplicons were absent, the signals stayed nearly undisturbed (Fig. S1D). For studying the selectivity, the designed assay was used to detect other interfering respiratory viruses, such as SARS-CoV, MERS-CoV, influenza A virus (IAV), and mouse hepatitis virus (MHV), bacteria and human cancer cells. As shown in Fig. S1E, only the SARS-CoV-2 samples had the significantly increased fluorescence intensities, indicating that the detection was highly selectivity without cross-reaction of non-SARS-CoV-2 targets. For RNA detection of SARS-CoV-2, the plasmids were transcribed to acquire nucleocapsid (N) RNA. Different concentrations of the RNA ranged from 1 to 10^7 aM were reversely transcribed and amplified. Then the detection of the transcribed RNA by Cas12a-crRNA complex was performed. As shown in Fig. S1F, along with the increase of SARS-CoV-2 N RNA concentrations, the fluorescence intensities rose up correspondingly. More, there was a linear relationship ($R^2 = 0.991$) between the fluorescence intensities and the RNA concentrations over the range from 1 to 10^7 aM (Fig. S1G).

3.3. CRISPR-Cas12a fluorescent assay for ultrasensitive and quantitative detection of SARS-CoV-2 pseudoviruses

Furthermore, to simulate SARS-CoV-2 detection, we produced lentiviruses harboring genomic fragments (N gene) of SARS-CoV-2. Viral titer was determined by qRT-PCR. The typical amplification plot and standard curve were shown in Fig. S2. According to the standard curve, the pseudovirus stock solution was about 1×10^8 copies/μL. Then, the fluorescent CRISPR-Cas12a assay was conducted. As shown in Fig. 2, the FL climbed up along with the increase of pseudoviral concentrations (Fig. 2A). There was a linear relationship ($R^2 = 0.987$) between fluorescence intensities and pseudoviral concentrations over the range from 10^0 to 10^8 copies per microliter (Fig. 2B) and the LOD was as low as 1 copy/μL (Fig. 2C). To compare with the classical method, qRT-PCR detection of N gene of SARS-CoV-2 was also conducted. The results revealed that the Ct values decreased as the increase of pseudoviral concentrations ranged from 10^0 to 10^8 copies/μL and the LOD of pseudoviruses was 1 copies/μL (Fig. 2D–F). The above-mentioned results indicated that the *trans*-cleavage of CRISPR-Cas12a could be leveraged for SARS-CoV-2 detection, and the performance of CRISPR-Cas12a fluorescent assay in our study was comparable with that of qRT-PCR.

3.4. CRISPR-Cas12a powered visual detection of SARS-CoV-2 pseudoviruses with a smartphone readout

In order to carry out effective detection of SARS-CoV-2 in resource-limited settings, we intended to develop a visual detection, which is independent of the microplate reader and could be easily read by a

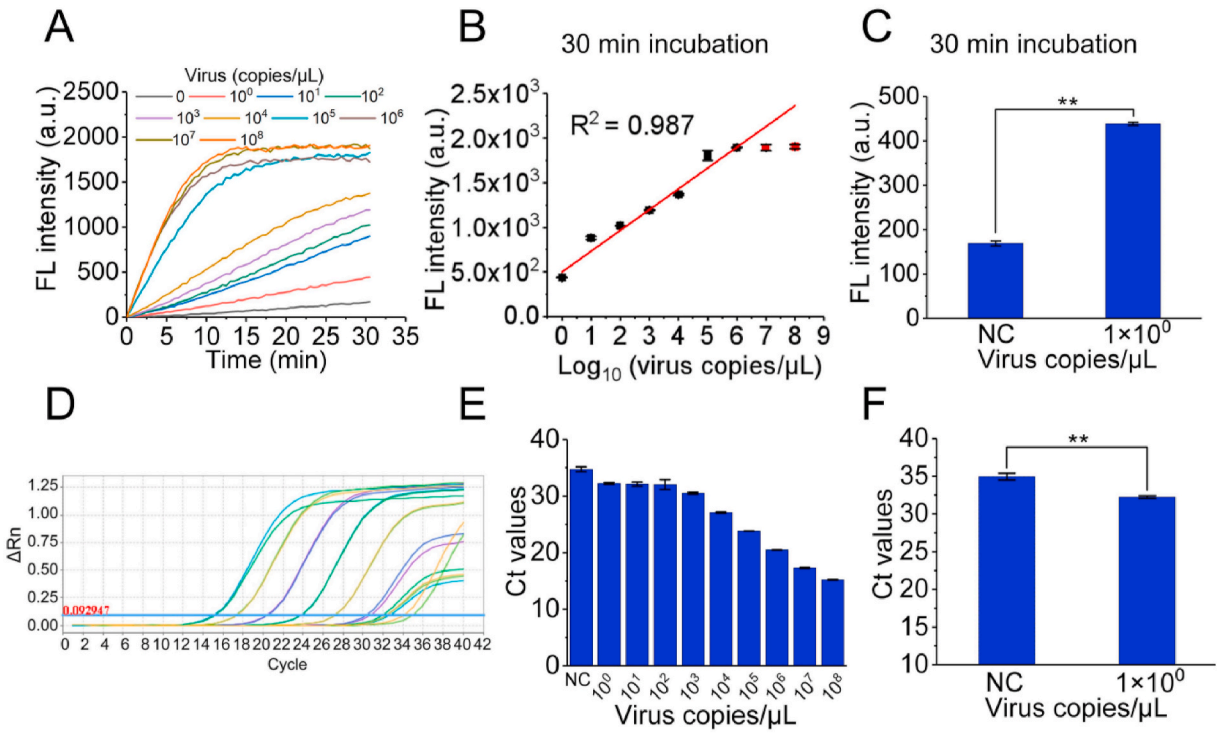

Fig. 2. The ultrasensitive detection of SARS-CoV-2-N pseudovirus in a and quantitative manner based on the *trans*-cleavage of CRISPR-Cas12a. (A) The real time FL for SARS-CoV-2-N pseudovirus detection. The FL comes from the CRISPR-Cas12a based *trans*-cleavage of a fluorescent ssDNA reporter. SARS-CoV-2-N RNA was extracted from the pseudoviruses and serially diluted. (B) The linear relationship between fluorescence intensities and SARS-CoV-2-N pseudovirus concentrations. (C) The LOD of SARS-CoV-2-N pseudoviruses detection based on *trans*-cleavage of CRISPR-Cas12a. (D–E) RT-qPCR detection of the SARS-CoV-2-N pseudoviruses. (F) The LOD of SARS-CoV-2-N pseudovirus detection using RT-qPCR. Data were obtained in triplicated and represented by mean ± SD. Two-tailed Student's t-test was used and $^{**}p < 0.01$.

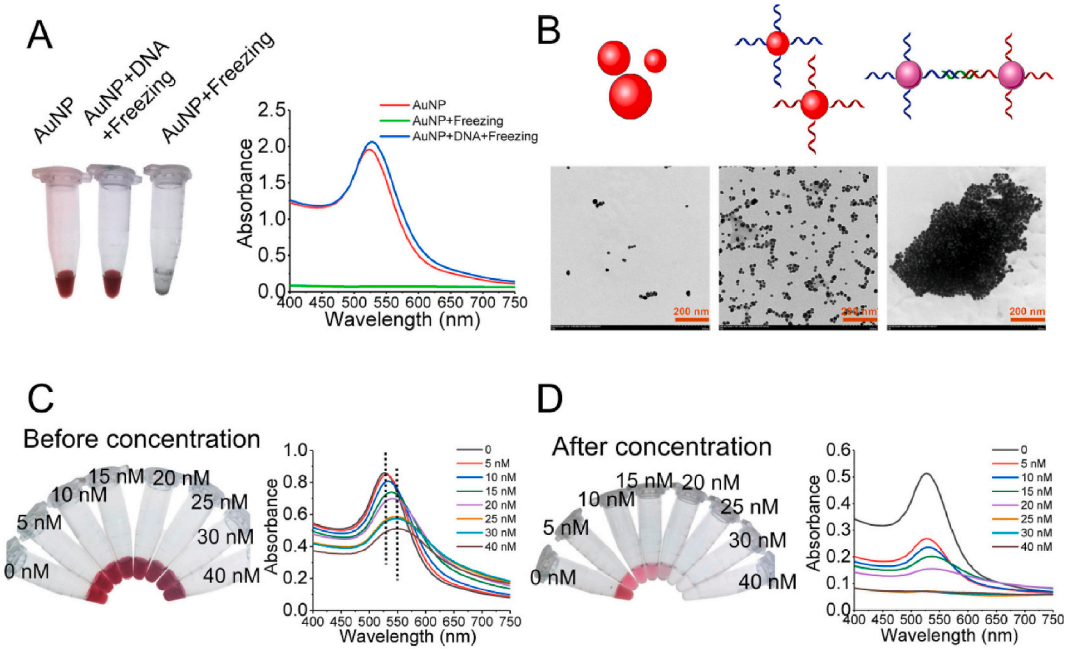

Fig. 3. The presence of linker ssDNA causes DNA hybridization resulting in the aggregation of AuNP-DNA probes. (A) Preparation of AuNP-DNA probes by the freezing method. The images of naked AuNPs without freezing, home-made AuNP-DNA probes via the freezing method and AuNPs after freezing (left panel) and their UV–Vis spectra (right panel). (B) The transmission electron microscope analysis of naked AuNPs (left), AuNP-DNA probes (middle), and cross-linked AuNP-DNA probes (right). (C, D) The color changes (left panel) and UV–Vis absorption spectroscopic analysis (right panel) of AuNP-DNA probes pairs with different concentrations of the linker ssDNA before and after centrifugation, respectively. (For interpretation of the references to color in this figure legend, the reader is referred to the Web version of this article.)

smartphone. It is demonstrated that aggregation and dispersion states of AuNPs display optical properties dependent of distances. This can be readily discerned by naked eyes. AuNPs and thiolated DNA (DNA1, sequence in Table S1) were conjugated by freezing at −20 °C for 2 h. As shown in Fig. 3A, after thawing, AuNPs solution mixed with thiolated DNA exhibited excellent stability and thus represented red color, which indicated that the AuNPs surface was successfully coated with the DNA probes. In contrast, the naked AuNPs solution aggregated to precipitate thoroughly after freezing. In addition, there was a 4 nm red-shift in terms of the absorption wavelength (4 nm) between the naked AuNPs and AuNP-DNA probes (Fig. 3A, right panel), indicating that the labeling was successfully achieved. The transmission electron microscope (TEM) analysis was further conducted to see the differences between aggregated and dispersed states of AuNPs (Fig. 3B). Then, the optimization of experimental conditions was carried out. Firstly, we determined the concentration of linker ssDNA that would be sufficient to cause complete cross-linking of AuNP-DNA probes pairs. In our experiment, we fixed the concentrations of AuNP-DNA1 and AuNP-DNA2 as 25 nM and varied the concentrations of linker ssDNA from 0 to 40 nM. As shown in Fig. 3C and D, the color transition could be observed at 5 nM and fully saturated at 25 nM. As 25 nM was the minimal concentration that resulted in a complete color transition; hence this concentration was used as the optimal parameter for the subsequent study. The reaction buffer was also optimized and it was observed that HEPES-buffered saline solution provided the highest signal to noise (S/N) ratio (Fig. S3), compared with other buffers. Thus HEPES-buffered saline solution was selected as the buffer for experiments.

At present, no validated reference material is available for SARS-

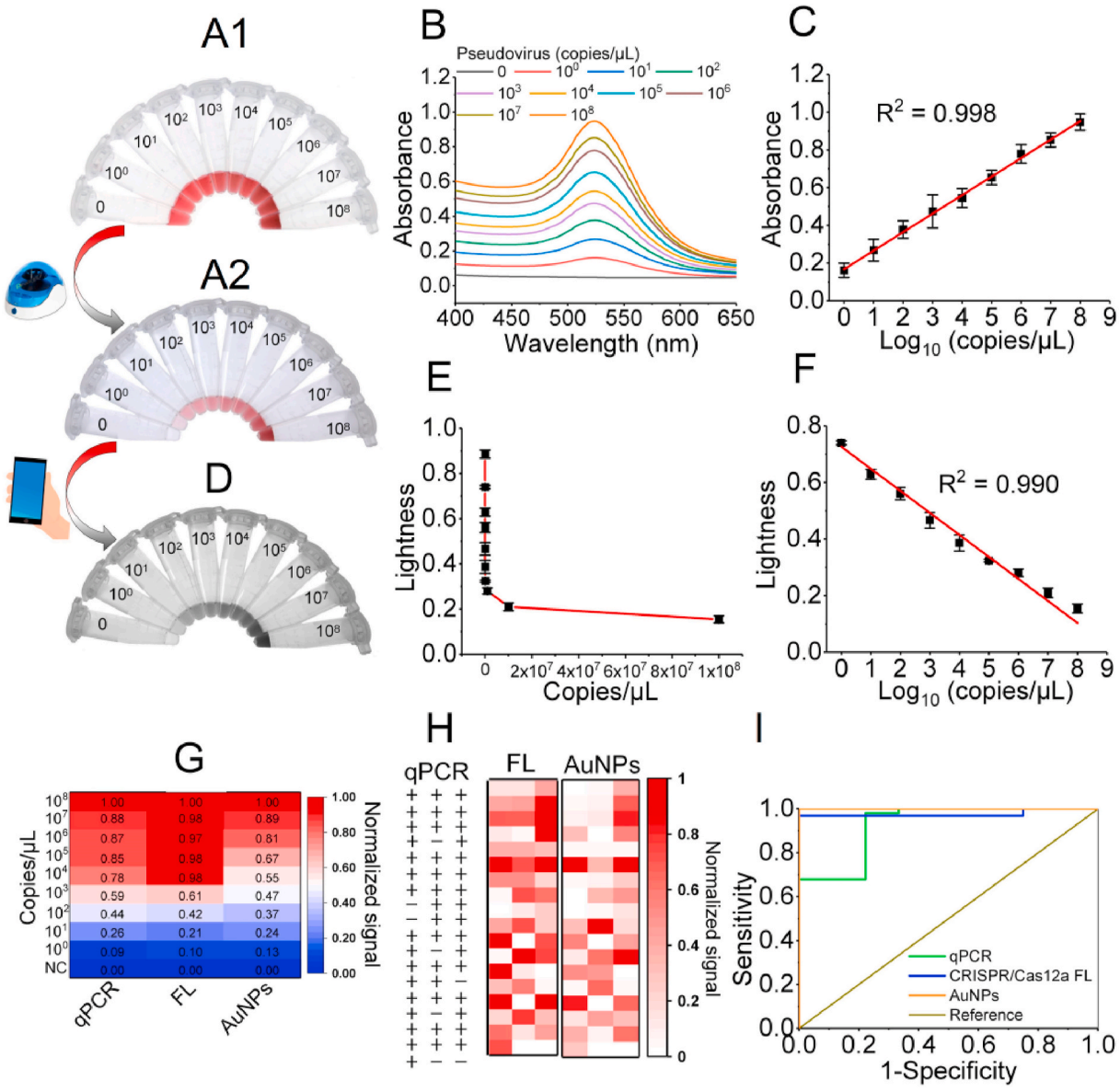

Fig. 4. CRISPR-Cas12a powered visual biosensor with a smartphone readout. Color transitions before (A1) and after mild centrifugation (A2) and corresponding UV–Vis spectroscopic data of A2 (B) of AuNP-DNA probes in the presence of pseudoviruses with various concentrations. (C) The linear relationship between UV–Vis absorbance and the concentrations of pseudoviruses. (D, E) Smartphone integrated detection of SARS-CoV-2. The RGB image was converted to a greyscale image (D) and analyzed offline using the Color Picker APP installed in the smartphone (E). (F) The linear relationship between lightness values and the concentrations of pseudoviruses. (G) The heat map showing the normalized results of three methods for SARS-CoV-2 pseudovirus detection. (H) Results for detection of SARS-CoV-2 in 54 samples using qPCR, CRISPR-Cas12a fluorescent and CRISPR-Cas12a powered visual biosensors. The "+" and "−" represent the positive and negative samples confirmed by qPCR, respectively. (I) ROC curve analysis of a double-blind validation cohort. (For interpretation of the references to color in this figure legend, the reader is referred to the Web version of this article.)

CoV-2 assays. WHO suggests for NAT (Nucleic Acid Test), one source of quantitated material in absence of an IS (International Standard) can be pseudotyped RNA viruses. In compliance with these instructions and requirements, we therefore tested our proposed biosensor with pseudoviruses containing SARS-CoV-2 N gene fragment. Upon the completion of optimization of the concentration of the linker ssDNA and reaction buffer, viral RNA extracted from the SARS-CoV-2 pseudoviruses was serially diluted and detected by the CRISPR-Cas12a powered visual biosensor. For the tube devoid of SARS-CoV-2 specific nucleic acids, the *trans*-cleavage of CRISPR-Cas12a was not activated, such that the linker ssDNA was supposed to induce the aggregation of AuNP-DNA probes. Therefore, after centrifugation, the supernatant was colorless. In contrast, the tube containing only 10^0 copy/μL pseudovirus displayed observable color change from colorless to red by naked eyes. Moreover, this biosensor seemed to display grades of color changes after centrifugation, dependent on the concentration of in a SARS-CoV-2, which suggested the capability of quantitative detection of SARS-CoV-2 (Fig. 4A). The LOD of the proposed biosensor for pseudoviruses was as low as 10^0 copies/μL. It is also intriguing to test the performance of amplification-free detection of SARS-CoV-2 pseudoviruses using the proposed biosensor. As shown in Fig. S5. The LOD went up to 10^6 copy/μL, a lot higher than that of amplification-adopted detection, indicating the necessity and importance of using pre-amplification technology for much improved sensitivity. Strong linear correlation ($R^2 = 0.998$) was obtained between the UV–Vis absorbance (Fig. 4B) and the concentrations of pseudoviruses ranged from 10^0 to 10^8 copies/μL (Fig. 4C). The RGB image was taken by a smartphone camera and then converted to a greyscale image (Fig. 4D) that was subsequently analyzed using the Color Picker App (Fig. S4). We noticed the HSL values and extracted the L (lightness) values corresponded to the concentrations of pseudoviruses (Fig. 4E). In terms of the lightness, black and white were defined as 0 and 1, respectively. As the results shown in Fig. 4F, there was an evident linear correlation ($R^2 = 0.990$) between lightness values and the concentrations of pseudoviruses ranged from 10^0 to 10^8 copies/μL. Next, we intended to compare the applicability of the aforementioned three detection methods. Different concentrations of the pseudoviruses ranged from 10^0 to 10^8 copies/μL were detected by qPCR, CRISPR-Cas12a fluorescent and CRISPR-Cas12a powered visual biosensors. The data were normalized and represented in Fig. 4G. All of the methods demonstrated the 10^0 copies/μL sensitivity. CRISPR-Cas12a powered visual biosensor showed better discrimination along with the increase of viral copies. Further, samples with or without SARS-CoV-2 pseudoviruses were detected with the three detection methods. The CRISPR-Cas12a fluorescent and visual biosensors both had 100% consistency with qPCR. (Fig. 4H). The receiver operating characteristic (ROC) curve of CRISPR-Cas12a powered visual biosensor demonstrated an AUC (Area Under the Curve) of 1.0, indicative of 100% for both of sensitivity and specificity (Fig. 4G). This 1.0 AUC value was better than that of qPCR (0.93) and CRISPR-Cas12a fluorescent biosensor (0.98). The sensitivity of our method was comparable or better in comparison to the recently developed CRISPR-Cas12a based SARS-CoV-2 detection (summarized in Table S2). In addition, our method was able to achieve semi-quantitative or quantitative detection of SARS-CoV-2 via endpoint absorbance, which can be realized by smartphone-based quantification. As previously reported, the lateral flow CRISPR-Cas assays compromised the sensitivity and had higher LOD values. For fluorescence-based CRISPR-Cas assays, they were easy-to-use and rather sensitive; however, such methods required a "cutoff" value to decide a sample, which was sometimes technically difficult to handle in practice. When referring to qPCR method for SARS-CoV-2 detection, it had some intrinsic shortcomings. Similar to fluorescent readouts, it was frequently encountered with "grey zone" issue, where the Ct value was too "vague" to judge a sample especially for the ones with fairly low viral loads. This led to false negatives or false positives (Huang et al., 2020). Our method, in this regard, balanced the sensitivity, accuracy and POC detection potentials. It had the LOD value of 1 copy/μL and it was able to eliminate detection uncertainty by generating chromogenic result at even single copy level.

The repeatability and reproducibility of the proposed CRISPR-Cas12a powered visual biosensor were both examined through analysis of the SARS-CoV-2 pseudoviruses samples (n = 10), as shown in Fig. S6. The lightness obtained using Color Picker App and the absorbance obtained by colorimetric measurement were both investigated and the relative standard deviations (RSD) values were acquired correspondingly. All calculated RSD values for repeatability and reproducibility were less than 6%, indicative of acceptable repeatability and reproducibility. The repeatability and reproducibility are crucial in biosensor development. It is generally recommended that RSD value less than 10% is the prerequisite to validate the reliability of developed biosensors (Ghorbanizamani et al., 2021).

It is can be assumed that some factors such as camera and light conditions would exert influences on photo acquisition and quality, resulting in discrepancies in detected results. We therefore used two different smartphone cameras (13 and 64 megapixels) and adopted two kinds of light modes (natural daylight and room lamp light) to investigate this. As shown in Fig. S7, although different camera and light conditions manifested slight variations, they were not statistically significant. This suggested the possibility to perform the diagnostics with the proposed biosensor with different smartphones and varying light conditions.

Lastly, we also did a comparison of two situations, namely adopting two individual steps (including CRISPR-Cas12a *trans*-cleavage and AuNPs incubation) and that of combining them into one-pot. The biosensor only outputted less than a half of the original absorbance value after merging the two steps together (Fig. S8). Hence, one-pot reaction strategy were not recommended. Apart from PCR, we also considered RPA for gene amplification. On one hand, RPA was exempted from thermal cycler, with more adaptability in POCT; on the other hand, as shown in Fig. S9, it generated much fewer incremental signals upon the addition of the targets. These reasons justified us in using PCR in amplification.

3.5. *CRISPR-Cas12a powered visual biosensor for SARS-CoV-2 detection in clinical bio-samples*

Further, we tested the diagnostic potential of CRISPR-Cas12a powered visual biosensor in clinical specimens. 50 clinical respiratory samples in total were included in the detection, which consisted of 20 COVID-19 cases and 30 samples from healthy subjects (all officially validated by the Tianjin CDC, China). The RNA samples were reversely transcribed and amplified with conventional PCR. Then, the PCR products were tested by CRISPR-Cas12a powered visual biosensor. As shown in Fig. 5A and B, our detection results had 100% agreement for both positive and negatives relative to the results obtained by qPCR. The quantified colorimetric signals of CRISPR-Cas12a visual biosensor (Fig. 5D) correctly identified and differentiated 50 positive and negative samples. This showed 100% agreement with the results from qPCR as shown in the Venn diagram (Fig. 5C).

4. Summary and conclusions

In summary, we reported a CRISPR-Cas12a powered visual biosensor for ultrasensitive detection of SARS-CoV-2. The colorimetric readouts could be discerned by naked eyes and could be analyzed directly by a smartphone installed with the Color Picker App, which greatly improved the simplicity, cut the cost and enhanced the detection portability. There was a linear relationship between the UV–Vis absorbance and the concentrations of pseudoviruses ranged from 10^0 to 10^8 copies/μL, with the LOD of SARS-CoV-2 pseudoviruses detection researching 1 copy/μL. Our designed biosensor was substantiated to be highly specific. The biosensor was further challenged by 20 positive and 30 negative clinical swab samples and it can be proved that this biosensor had 100% agreement with qPCR results. The "pull-down" method used in the

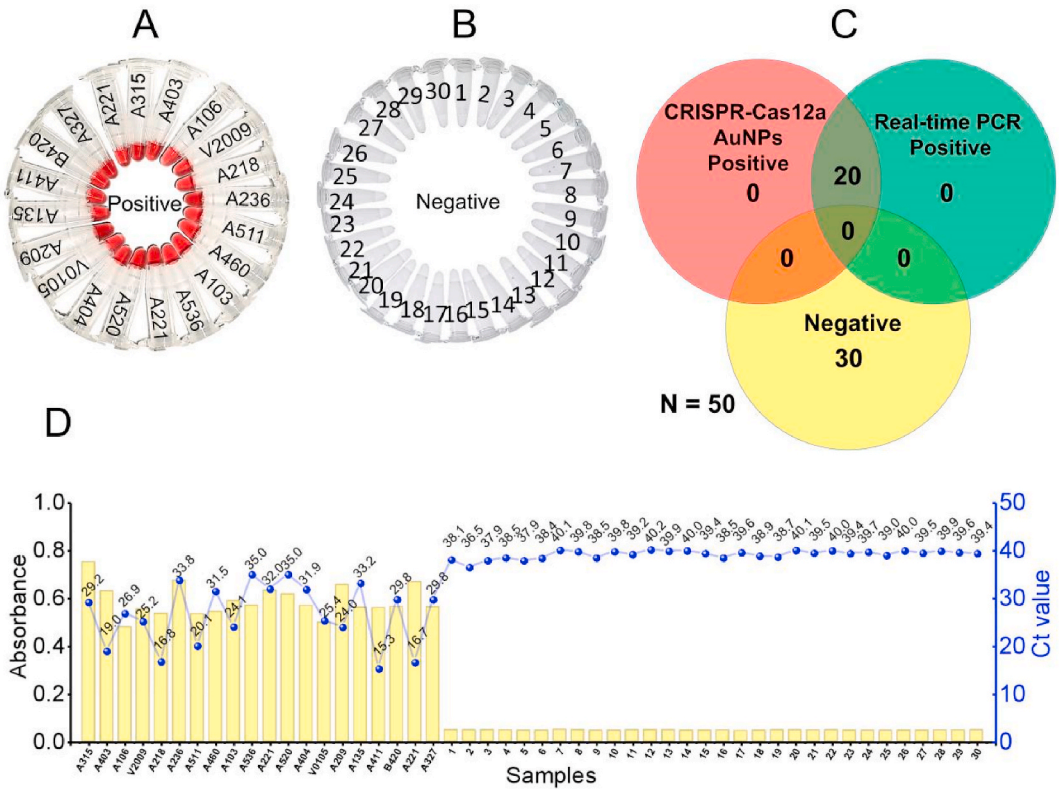

Fig. 5. CRISPR-Cas12a powered visual biosensor for SARS-CoV-2 detection of clinical bio-samples. (A and B) 50 clinical bio-samples (20 positive samples and 30 negative samples) were detected with the proposed CRISPR-Cas12a visual biosensor. All 20 positive samples have obvious color changes to red, while the negative samples remain colorless. (C) The Venn diagram shows the consistency between the CRISPR-Cas12a powered visual biosensor and qPCR assay. (D) The absorbance ($A_{526\ nm}$) of samples at detected by the proposed biosensor and their corresponding Ct values of qPCR. (For interpretation of the references to color in this figure legend, the reader is referred to the Web version of this article.)

proposed biosensor has been similarity used in a couple previous publications (Cao et al., 2021; Hu et al., 2020; Jiang et al., 2021; Li et al., 2020; Yuan et al., 2020; Zhang et al., 2021; Zhou et al., 2020). Our work was inspired by them and but it has its own advantages. Simply put, we introduced an extra centrifugation step, which can be easily done by a handheld centrifuge. This gave a sharper discrimination for the "pull--down" samples, resulting a single-copy resolution for SARS-CoV-2 detection by naked eyes. Also, in order to reduce user bias in interpreting in-tube readout results, we applied a smartphone App-enabled in-tube readout that used the built-in camera to capture the images the illuminated reaction tubes, which gave a "handle" for semi-quantitative detection. However, the proposed biosensor, as other methods, may suffer from some limitations. The PCR method for gene amplification still requires thermal cyclers, which is one step away from POC detection. The solution to this could be to replace PCR by some isothermal amplification technology such as recombinase polymerase amplification (RPA) and loop-mediated isothermal amplification (LAMP). In addition, the proposed biosensor contained several steps, these multistep liquid transfer could be further integrated into a one-pot reaction in potential by automation, minimal instrumentation or a simplified process (Arizti-Sanz et al., 2020).

The above-mentioned limitations could be further investigated and solved by the future work. In conclusion, our proposed biosensor provided an ultrasensitive, specific, simple and visualized detection of SARS-CoV-2, which could be deployable to the fields in potential.

Our work not only expands the reaching of CRISPR-Cas technology in biosensing but also it, as an alternative to the long-standing qPCR method, could be further explored to put into real practice in the near future.

Credit authorship contribution statement

Long Ma: Conceptualization, Investigation, Project Management, Supervision, Methodology, Writing-original draft, Writing-review & editing, Funding acquisition. Lijuan Yin: Supervision, Investigation, Data analysis, Writing-original draft, Writing-review & editing. Xiaoyan Li: Clinical samples. Si Chen: Experiment, data analysis. Lei Peng: Experiment, data analysis. Guozhen Liu: Writing-review & editing. Shengying Ye: Wenlu Zhang: Experiment. Shuli Man: Project Management, Investigation, Writing-review & editing.

Declaration of competing interest

The authors declare that they have no known competing financial interests or personal relationships that could have appeared to influence the work reported in this paper.

Acknowledgments

This work was financially supported by National Natural Science Foundation of China (No. 32072309, 21672161, 81503086), Tianjin Municipal Science and Technology Committee (19JCYBJC27800) and State Key Laboratory of Food Nutrition and Safety, Tianjin University of Science & Technology (19PTSYJC00060). We thank Prof. Fei Guo and Siqi Hu for providing us with their plasmid encoding H1N1 influenza A virus nucleocapsid/NP protein. We thank Prof. Zhaohui Qian and Xiuyuan Ou for providing us with their plasmids encoding SARS-CoV, MERES-CoV and MHV N proteins. All of the four professors are from Chinese Academy of Medical Sciences & Peking Union Medical College.

Appendix A. Supplementary data

Supplementary data to this article can be found online at https://doi.org/10.1016/j.bios.2021.113646.

References

Abudayyeh, O.O., Gootenberg, J.S., Konermann, S., Joung, J., Slaymaker, I.M., Cox, D.B. T., Shmakov, S., Makarova, K.S., Semenova, E., Minakhin, L., Severinov, K., Regev, A., Lander, E.S., Koonin, E.V., Zhang, F., 2016. Science 353, aaf5573.

Ahmadivand, A., Gerislioglu, B., Ramezani, Z., Kaushik, A., Manickam, P., Ghoreishi, S. A., 2021. Biosens. Bioelectron. 177, 112971.

Arai, S., Krisztˊ, R., Harada, K., Looi, L.S., Matsuda, S., Wongso, D., Suo, S., Ishiura, S., Tseng, Y.H., Raghunath, M., Ito, T., Tsuboi, T., Kitaguchi, T., 2018. Angew. Chem. Int. Ed. 57, 10873–10878.

Arizti-Sanz, J., Freije, C.A., Stanton, A.C., Petros, B.A., Boehm, C.K., Siddiqui, S., Shaw, B.M., Adams, G., Kosoko-Thoroddsen, T.-S.F., Kemball, M.E., Uwanibe, J.N., Ajogbasile, F.V., Eromon, P.E., Gross, R., Wronka, L., Caviness, K., Hensley, L.E., Bergman, N.H., MacInnis, B.L., Happi, C.T., Lemieux, J.E., Sabeti, P.C., Myhrvold, C., 2020. Nat. Commun. 11, 5921.

Barrangou, R., Fremaux, C., Deveau, H., Richards, M., Boyaval, P., Moineau, S., Romero, D.A., Horvath, P., 2007. Science 315, 1709–1712.

Broughton, J.P., Deng, X., Yu, G., Fasching, C.L., Servellita, V., Singh, J., Miao, X., Streithorst, J.A., Granados, A., Sotomayor-Gonzalez, A., Zorn, K., Gopez, A., Hsu, E., Gu, W., Miller, S., Pan, C., Guevara, H., Wadford, D.A., Chen, J.S., Chiu, C.Y., 2020. Nat. Biotechnol. 38, 870–874.

Cao, Y., Wu, J., Pang, B., Zhang, H., Le, X.C., 2021. Chem. Commun. 57, 6871–6874.

Chang, C.-C., Chen, C.-P., Wu, T.-H., Yang, C.-H., Lin, C.-W., Chen, C.-Y., 2019. Nanomaterials-Basel 9, 861.

Chen, J.S., Ma, E., Harrington, L.B., Da Costa, M., Tian, X., Palefsky, J.M., Doudna, J.A., 2018. Science 360, 436–439.

Chen, M., Luo, R., Li, S., Li, H., Qin, Y., Zhou, D., Liu, H., Gong, X., Chang, J., 2020. Anal. Chem. 92, 13336–13342.

Corman, V.M., Landt, O., Kaiser, M., Molenkamp, R., Meijer, A., Chu, D.K., Bleicker, T., Brünink, S., Schneider, J., Schmidt, M.L., Mulders, D.G., Haagmans, B.L., van der Veer, B., van den Brink, S., Wijsman, L., Goderski, G., Romette, J.-L., Ellis, J., Zambon, M., Peiris, M., Goossens, H., Reusken, C., Koopmans, M.P., Drosten, C., 2020. Euro Surveill. 25, 2000045.

Ghorbanizamani, F., Moulahoum, H., Zihnioglu, F., Evran, S., Cicek, C., Sertoz, R., Arda, B., Goksel, T., Turhan, K., Timur, S., 2021. Quantitative paper-based dot blot assay for spike protein detection using fuchsine dye-loaded polymersomes. Biosens. Bioelectron. 192, 113484.

Gootenberg, J.S., Abudayyeh, O.O., Lee, J.W., Essletzbichler, P., Dy, A.J., Joung, J., Verdine, V., Donghia, N., Daringer, N.M., Freije, C.A., Myhrvold, C., Bhattacharyya, R.P., Livny, J., Regev, A., Koonin, E.V., Hung, D.T., Sabeti, P.C., Collins, J.J., Zhang, F., 2017. Science 356, 438–442.

Hu, M., Yuan, C., Tian, T., Wang, X., Sun, J., Xiong, E., Zhou, X., 2020. J. Am. Chem. Soc. 142, 7506–7513.

Huang, W., Yu, L., Wen, D., Wei, D., Sun, Y., Zhao, H., Ye, Y., Chen, W., Zhu, Y., Wang, L., Wang, L., Wu, W., Zhao, Q., Xu, Y., Gu, D., Nie, G., Zhu, D., Guo, Z., Ma, X., Niu, L., Huang, Y., Liu, Y., Peng, B., Zhang, R., Zhang, X., Li, D., Liu, Y., Yang, G., Liu, L., Zhou, Y., Wang, Y., Hou, T., Gao, Q., Li, W., Chen, S., Hu, X., Han, M., Zheng, H., Weng, J., Cai, Z., Zhang, X., Song, F., Zhao, G., Wang, J., 2020. EBioMedicine 61, 103036.

Jans, H., Huo, Q., 2012. Chem. Soc. Rev. 41, 2849–2866.

Jiang, Y., Hu, M., Liu, A.-A., Lin, Y., Liu, L., Yu, B., Zhou, X., Pang, D.-W., 2021. ACS Sens. 6, 1086–1093.

Kaminski, M.M., Abudayyeh, O.O., Gootenberg, J.S., Zhang, F., Collins, J.J., 2021. CRISPR-based diagnostics. Nat. Biomed. Eng. 5, 643–656.

Li, S., Cheng, Q., Wang, J., Li, X., Zhang, Z., Gao, S., Cao, R., Zhao, G., Wang, J., 2018. Cell Discov 4, 20.

Li, Y., Li, S., Wang, J., Liu, G., 2019a. CRISPR/Cas systems towards next-generation biosensing. Trends Biotechnol. 37, 730–743.

Li, Y., Mansour, H., Wang, T., Poojari, S., Li, F., 2019b. Anal. Chem. 91, 11510–11513.

Liu, J., Lu, Y., 2006. Nat. Protoc. 1, 246–252.

Morales-Narváez, E., Dincer, C., 2020. Biosens. Bioelectron. 163, 112274.

Patchsung, M., Jantarug, K., Pattama, A., Aphicho, K., Suraritdechachai, S., Meesawat, P., Sappakhaw, K., Leelahakorn, N., Ruenkam, T., Wongsatit, T., Athipanyasilp, N., Eiamthong, B., Lakkanasirorat, B., Phoodokmai, T., Niljianskul, N., Pakotiprapha, D., Chanarat, S., Homchan, A., Tinikul, R., Kamutira, P., Phiwkaow, K., Soithongcharoen, S., Kantiwiriyawanitch, C., Pongsupasa, V., Trisrivirat, D., Jaroensuk, J., Wongnate, T., Maenpuen, S., Chaiyen, P., Kamnerdnakta, S., Swangsri, J., Chuthapisith, S., Sirivatanauksorn, Y., Chaimayo, C., Sutthent, R., Kantakamalakul, W., Joung, J., Ladha, A., Jin, X., Gootenberg, J.S., Abudayyeh, O.O., Zhang, F., Horthongkham, N., Uttamapinant, C., 2020. Nat. Biomed. Eng. 4, 1140–1149.

Peng, L., Zhou, J., Yin, L., Man, S., Ma, L., 2020. Anal. Chim. Acta 1125, 162–168.

Quesada-González, D., Merkoçi, A., 2017. Biosens. Bioelectron. 92, 549–562.

Wu, H., Chen, X., Zhang, M., Wang, X., Chen, Y., Qian, C., Wu, J., Xu, J., 2021. Trac. Trends Anal. Chem. 135, 116150.

Yin, L., Man, S., Ye, S., Liu, G., Ma, L., 2021. Biosens. Bioelectron. 193, 113541.

Yuan, C., Tian, T., Sun, J., Hu, M., Wang, X., Xiong, E., Cheng, M., Bao, Y., Lin, W., Jiang, J., Yang, C., Chen, Q., Zhang, H., Wang, H., Wang, X., Deng, X., Liao, X., Liu, Y., Wang, Z., Zhang, G., Zhou, X., 2020. Anal. Chem. 92, 4029–4037.

Zagorovsky, K., Chan, W.C., 2013. Angew. Chem. Int. Ed. 52, 3168–3171.

Zhang, W.S., Pan, J., Li, F., Zhu, M., Xu, M., Zhu, H., Yu, Y., Su, G., 2021. Anal. Chem. 93, 4126–4133.

Zhao, W., Brook, M.A., Li, Y., 2008. Chembiochem 9, 2363–2371.

Zhou, J., Yin, L., Dong, Y., Peng, L., Liu, G., Man, S., Ma, L., 2020. Anal. Chim. Acta 1127, 225–233.

Zhou, R., Li, Y., Dong, T., Tang, Y., Li, F., 2020. Chem. Commun. 56, 3536–3538.

Zhu, N., Zhang, D., Wang, W., Li, X., Yang, B., Song, J., Zhao, X., Huang, B., Shi, W., Lu, R., Niu, P., Zhan, F., Ma, X., Wang, D., Xu, W., Wu, G., Gao, G.F., Tan, W., 2020. N. Engl. J. Med. 382, 727–733.